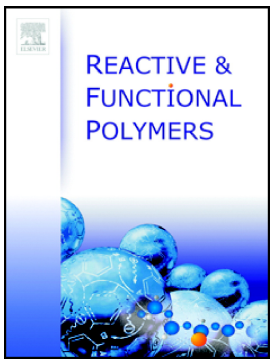

PLA-based functionally graded laminates for tunable controlled release of carvacrol obtained by combining electrospinning with solvent casting

Roberto Scaffaro, Andrea Maio, Emmanuel F. Gulino, Giorgio D.M. Micale

PII: S1381-5148(19)31170-8

DOI: https://doi.org/10.1016/j.reactfunctpolym.2020.104490

Reference: REACT 104490

To appear in: *Reactive and Functional Polymers*

Received date: 5 November 2019

Revised date: 7 January 2020

Accepted date: 11 January 2020

Please cite this article as: R. Scaffaro, A. Maio, E.F. Gulino, et al., PLA-based functionally graded laminates for tunable controlled release of carvacrol obtained by combining electrospinning with solvent casting, *Reactive and Functional Polymers* (2019), https://doi.org/10.1016/j.reactfunctpolym.2020.104490

PLA-based functionally graded laminates for tunable controlled release of carvacrol obtained by combining electrospinning with solvent casting

Roberto Scaffaro* roberto.scaffaro@unipa.it, Andrea Maio, Emmanuel F. Gulino, Giorgio D.M. Micale.

Department of Engineering, University of Palermo, Viale delle Scienze Ed. 6, 90128 Palermo, Italy
*Corresponding author.

Abstract

A novel approach was designed to fabricate high-added value manufacts, starting from cost-effective materials and combining well-known processing techniques.

Bi- and three-layered, functionally graded laminates were achieved by direct electrospinning onto dense substrates. The architecture of each multilayer comprises a dense layer formed by solvent casting, which is constituted by polylactic acid (PLA) and carvacrol, and one or two electrospun fibrous skin layers, consisting of PLA only. Processing-structure-properties relationships of such materials were investigated.

As regards mechanical behavior, the amount of fibrous PLA layers determined an increase of stiffness from 20 to 35 MPa, adequately predicted by isostrain model, whereas the breaking properties proved to be governed by the dense layer, with values of tensile strength (6 MPa) and elongation at break (200%) almost ten-folded with respect to those of electrospun fibrous PLA.

As concerns carvacrol release behavior, the presence of fibrous skin, especially in three-layered structures, proved to progressively reduce the burst delivery at early stage of immersion, while enhancing the depletion time, i.e. the release activity, of such devices from 288 to 795 hours. Furthermore, a correlation was found between the thickness of fibrous layers and release kinetics, thus suggesting that adjusting simple variables, such as electrospinning time, allows to control the ultimate properties of these devices. Moreover, this approach enables gathering the mechanical robustness of a dense film with the extremely large specific area of fibrous materials, thus showing promising potential for a broad range of application fields.

Keywords: Electrospinning onto film; Solvent casting; functionally graded; Peppas model; Controlled drug release; Multilayer.

1. Introduction

Polymer-based materials with well-orchestrated morphologies are an emerging class of materials that currently find application in many fields, including regenerative medicine, drug delivery, bioprocess intensification, electrochemistry**,** textiles, smart packaging, sensing, desalination, filtration processes [1–6]. However, high surface area, hierarchical structure, and ordered pores architecture are difficult to be simultaneously satisfied and managed using one polymer or one processing technique [2,7].

Usually, graded structures, characterized by either discrete or uniform variation of a given property, are obtained by time consuming protocols or multi-component formulations, whose overall optimization and control are hard to manage [7].

Combining different processes may enable the possibility to optimize separately multiple variables for achieving modular properties, and/or to provide multiple processing options by gathering the strengths of each processing technique in the perspective of expanding applications.

The basic idea is that the combined processing approach may improve the preparation of functional materials, starting from cost-effective materials and well known processing techniques, opportunely combined each other.

Herein, it is reported a simple strategy to prepare polymeric laminates with tunable morphology and functionality, by using two quite common and relatively inexpensive materials, such as a commercial poly(lactic acid) (PLA), extremely widespread in the scientific literature by virtue of its biocompatibility, renewability and biodegradability, and an essential oil, i.e. carvacrol (CRV), which recently stimulated a growing interest as a natural antimicrobial, antioxidant and antitumor agent [8,9]. More in detail, the aim is to demonstrate the possibility to achieve different types of graded structures constituted by a dense, layer of PLA containing carvacrol (used as a model molecule) and one or two fibrous skins made by PLA only, via the coupling of solvent casting and electrospinning methods. The effect of this surface treatment on mechanical and *in vitro* release properties of resulting materials, as well as the possibility to tune such target properties by modulating operating variables will be discussed and the strong processing-structure-property relationship investigated is supposed to provide guidance for extending the combined processing approach to as many as possible application fields. In fact, these systems may hold tremendous potential in long-term topical treatment of infections located in interstitial/contact tissues, including buccal mucosa, vulvovaginal and gingival disorders [10–14].

2. Experimental part

2.1 Materials and chemicals

The raw materials used in this work were a sample of PLA 2002D (Mw 215 kDa; D-lactide content 4%), purchased from NatureWorks, a liquid sample of CRV (2-methyl-5-(1-methylethyl)-phenol, melting temperature=1 °C, density=0.977 g/L, purity ≥97%), supplied chloroform (CF), Acetone (Ac), and phosphate-saline buffer (PBS) were purchased from Sigma Aldrich. All the reactants were used as received.

2.2 Preparation route

Figure 1 provides the schematics of the combined processing approach adopted in this work. Thin films containing 86 wt.% PLA and 14 wt.% CRV were fabricated by solvent casting. More in detail, CRV (976.7 mg) was added dropwise to 60 mL of CF:Ac (2:1 by volume), thereafter 6 g of PLA were added to the solution and totally dissolved by stirring overnight. Thin films were achieved by pouring the solution onto rotary glass cylinders having ultra-smooth surface. This protocol allows fabricating films with extremely uniform thickness (30±1 μm) without irregularities nor pores. Among these, films having average thickness values as similar as possible to each other have been selected, cut into rectangular foils (120 mm x 78.5 mm), weighed and rolled-up onto an Al-coated rotary collector having diameter=25 mm, for the subsequent electrospinning operations, which were performed as follows.

PLA (2 g) was dissolved in 20 mL of a CF/Ac (2:1 by volume) solvent mixture and homogenized in the same conditions as those used for fabricating thin films, thereafter such solution was fed to a glass syringe and electrospun, thereby being deposited onto one side or both the sides of films. The process was carried out at T=25 °C and 40% relative humidity in a conventional electrospinning unit (Linari Engineering-Biomedical Division, Italy) equipped with a multi-needle spinneret, having 12 stainless steel needles (19-gauge), parallel to each other, with an inter-needle distance equal to 50 mm. The following parameters were selected: flow rate=2 mL/h; tip-to-collector distance=15 cm; supplied high voltage=15 kV; mandrel rotating speed=5 rpm. Furthermore, by changing electrospinning time from 5 to 10 minutes it was possible to obtain three-layer samples with different morphological structures. The four samples prepared in the frame of this work were coded as follows:

ML: a monolayer dense film prepared by solvent casting containing PLA+14% CRV

BL: a bilayer structure, constituted by a dense film containing PLA+14% CRV and a PLA fibrous membrane prepared by electrospinning for 5 mins.

TL-5: a three-layer structure, constituted by an inner dense film containing PLA+14% CRV and two outer PLA-based fibrous membranes prepared by electrospinning for 5 mins.

TL-10: a three-layer film constituted by an inner dense film containing PLA+14% CRV and two outer PLA fibrous membranes prepared by electrospinning for 10 mins.

The pictorial representation of the different structures achieved can be observed in **Figure 1**. Basically, by coupling electrospinning with solvent casting, it was possible achieving bilayer and three-layer skin-core-skin structures, being constituted by an identical dense core and one or two fibrous skins.

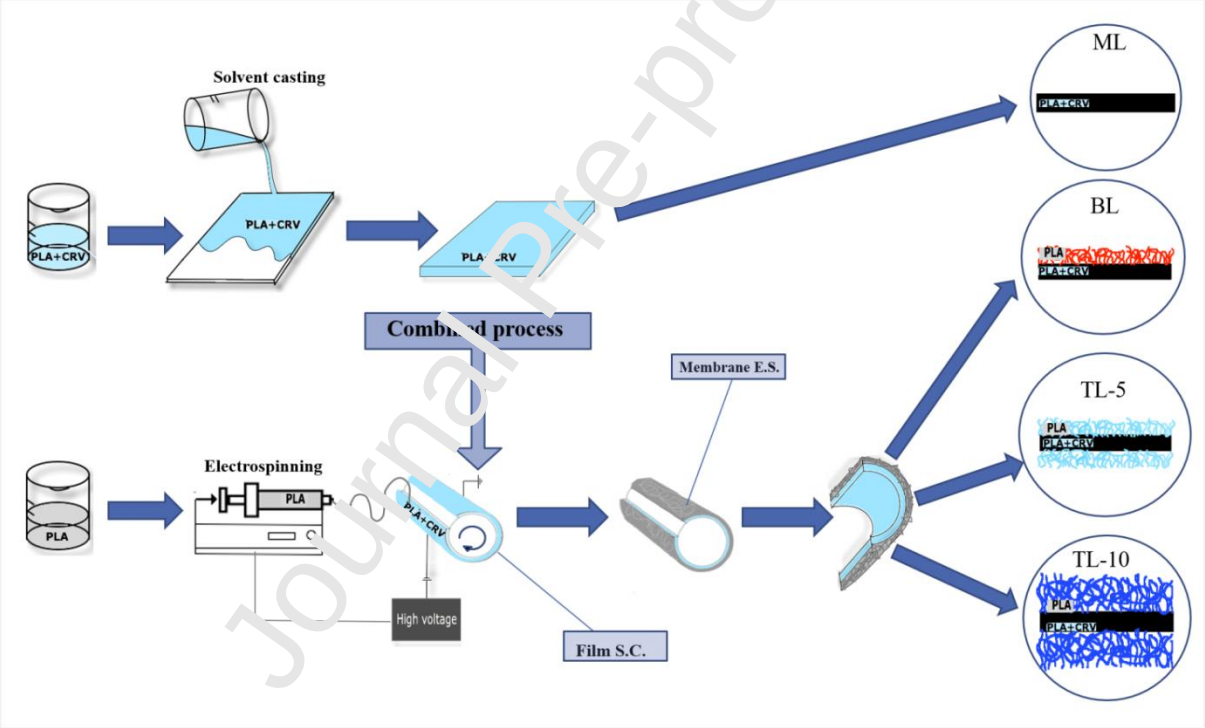

Figure 1. Schematics of the process

Table 1 reports the main properties of ML, BL, TL-5 and TL-10. All of the samples display the same nominal CRV content, since it is present only in the dense core, common for all the samples, while differing each other for the mass of fibrous layer(s) deposited, with ensuing different nominal CRV concentrations and fibers/film weight ratios, which have been esteemed, being known the formulation, by weighing the samples before and after the coating.

Table 1. Main properties of ML, BL, TL-5, TL-10

Sample	mass of dense layer (mg)	Mass of fibrous layer(s) (mg)	Nominal CRV content (mg)	Nominal CRV concentration (wt.%)	fibers/film weight ratio
ML	340.2	0	47.6	14%	0
BL	340.7	204	47.7	8.85%	0.58
TL-5	340.1	369	47.6	6.71%	1.08
TL-10	339.4	806	47.5	4.15%	2.37

As control, electrospun membranes and dense cast films of neat PLA, respectively coded as ES-PLA and SC-PLA, were prepared in the same conditions.

2.3 Characterization

Scanning electron microscopy (SEM) analysis was carried out by using an ESEM FEI QUANTA 200 (Thermo Fisher Scientific, USA) onto both surface and cross-section of each sample. An open source image processing software (Image J) equipped with a plug-in (Diameter J) was used to evaluate the features of fibrous layers, such as diameter size distribution and mean size of the fibers.

Water contact angle (WCA) measurements were carried out at room temperature by using an FTA 1000 (First Ten Ångstroms, UK) instrument. 4 μL of deionized water were dropped onto the surface of each sample by way of an automatic liquid drop dosing system. Images of the drop on the surface were acquired after 20 s.

Tensile tests were performed to evaluate the mechanical properties of the samples, by using an Instron 3365 (Instron, Norwood, MA, USA) universal testing machine, operating at a crosshead speed of 1 mm/min until 3 minutes; thereafter, the crosshead speed was increased to 100 mm/min until specimen failure. Tensile tests were carried out onto prismatic-shaped specimens, obtained by die-cutting (Tecnofustelle, Italy). All the specimens had width=10 mm and length=90 mm (gauge length=30 mm), while differing each other for the thickness, which was measured prior to each experimental run. Volume fraction of fibrous layer(s) was esteemed by subtracting the thickness of dense layer (equal to 30 μm) from that of the entire sample.

Elastic modulus (E) was calculated as initial slope of stress-strain curves, extrapolated at zero-strain, tensile strength (TS) and elongation at break were respectively evaluated as the maximum values of stress and strain for each curve. For each experimental run, at least 10 replicates were tested, and the data were provided as mean values with standard deviations.

FTIR/ATR tests were performed by a Perkin-Elmer FT-IR/NIR Spectrum 400 spectrophotometer, spectra were collected in the range 4000-400 cm^{-1}.

Release tests were carried out in PBS at 37 °C up to 550 h to assess the CRV release, calculated by monitoring the absorbance peak at 273 nm via a UV-vis Specord 252 spectrophotometer (Analytik Jena, Jena, Germany). Prior to release tests, a series of PBS solutions with known CRV concentrations was used to construct a calibration curve, which correlates the absorbance peak intensity to the concentration. In the concentration range investigated (i.e. until 20 mg/dL), the calibration curve was found to be a line, whose best fitting was performed by the method of least squares. The release of carvacrol from the devices was investigated by immersing a pre-weighed sample (a disk with 25 mm diameter) in 10 mL of PBS and thereby monitoring at predetermined time intervals the absorbance of CRV of the storage solutions. Note that, after each measurement, the samples were immersed in fresh PBS to maximize the diffusion driving force. The cumulative release of CRV was thereby calculated by sequentially adding the amount released after each step.

2. Results and discussion

Figure 2 provides SEM micrographs of the cross sections of the samples prepared in this work. Cross-section of ML (panel A) displays a uniform thickness of about 30 μm with no aggregates, likely due to the good mutual affinity between PLA and CRV. BL sample morphology, reported in panel B, demonstrates the effectiveness of the combined processing herein proposed. In fact, it is clearly detectable the assembly of a fibrous layer onto the dense film. Moreover, the sample shows a uniform interface. Cross-section of TL-5 provided in Figure 2 C, displays a skin-core-skin structure, with a dense core sandwiched by two fibrous layers. TL-10 (Figure 2D) exhibits the same structure as TL-5 but in this latter case the thickness of outer fibrous layers drastically increased such that exceeding the hundreds of microns. Even in this case, a good and uniform interface was detected, with both fibrous layers perfectly adherent to the dense core. In order to get some information about mats architecture, SEM imaging was carried out even onto top side of each sample.

In **Figure 3 A-C** there are respectively reported the top views of fibrous surfaces of BL, TL-5 and TL-10, together with their diameter size distributions (DSD). Furthermore, in top right of panel A the smooth surface of ML is provided for sake of comparison. Note that for three-layers, DSD was evaluated onto both sides, to make sure there were no discrepancies between top and bottom side that may occur due to progressive changes upon increasing sample thickness in tip-to-collector distance and collector

conductivity, since PLA/CRV and PLA behave as electrical insulators. Notably, the architecture of fibrous mats was found to be extremely similar for all the samples, with a uniform and homogeneous coating of randomly oriented fibers. This approach ensures a high electrospinnability, since no beads or blobs phenomena were detected. Another relevant aspect is the uniformity of fibers, with all the samples presenting unimodal distributions, whose maxima were centered at 3 μm, and hence similar mean values, regardless of processing parameters. Furthermore, three-layer samples displayed the same features in both sides. Of course, due to the aforementioned presence of insulating layers, the mean diameter of fibers in the fibrous skins of bi- and three-layer devices was found to be slightly larger than that of ES-PLA (see Fig. S1-S2).

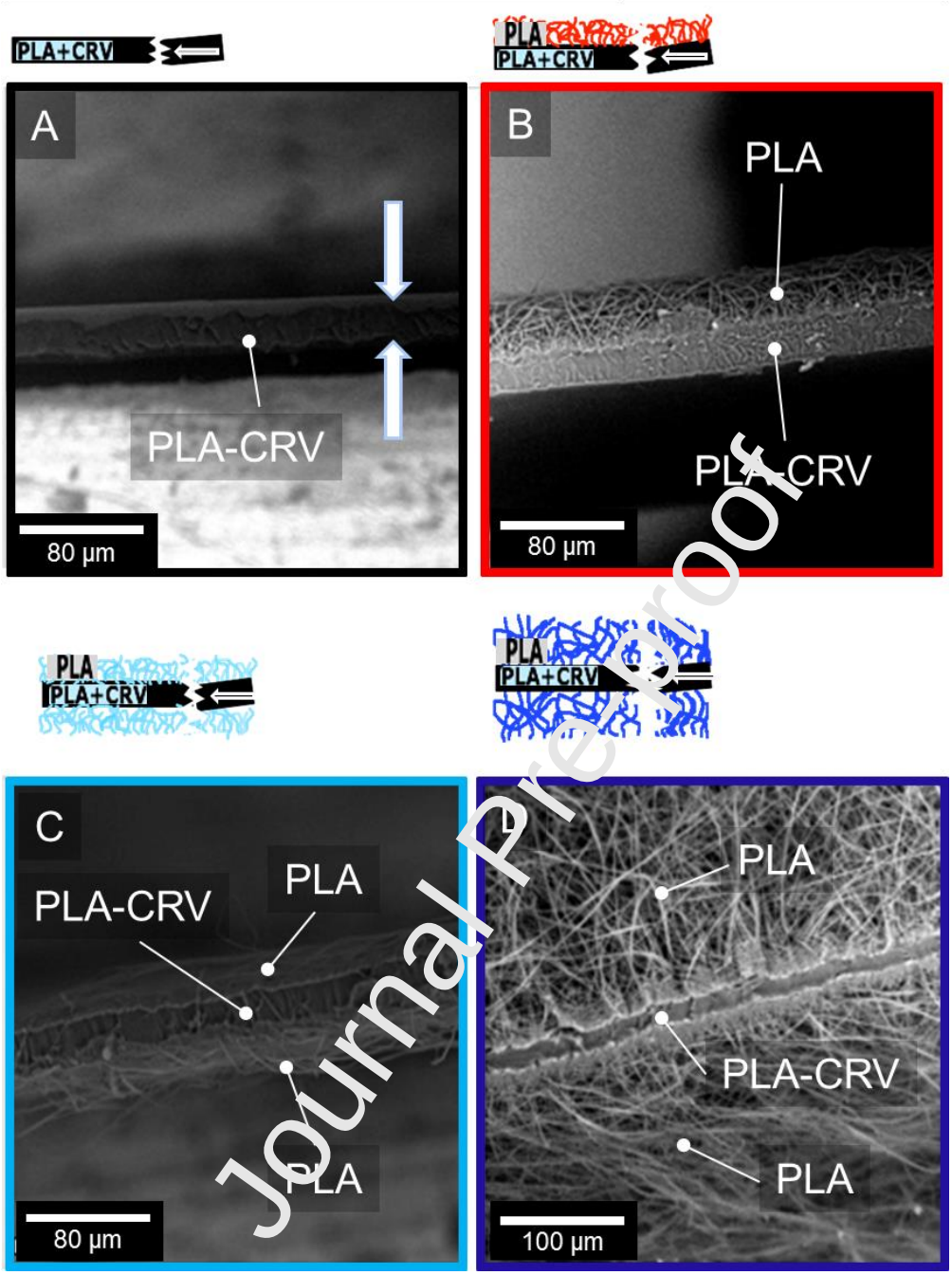

Figure 2. SEM micrographs of the cross-sections of ML (A), BL (B), TL-5 (C), TL-10 (D)

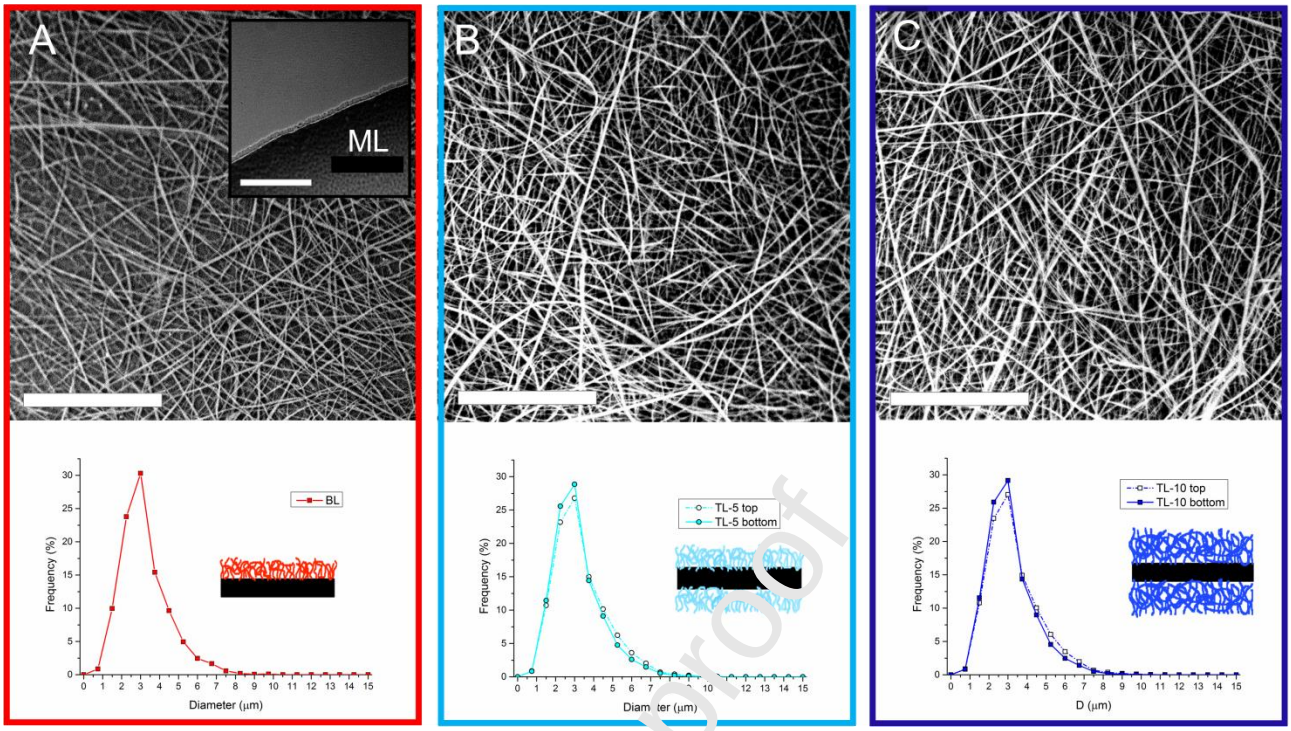

Figure 3. SEM micrographs reporting top views and diameter size distribution for BL (A), TL-5 (B) and TL-10 (C). Inset of panel A: surface view of reference ML. Note that in three-layer samples the diameter size distribution is provided for both the sides. Scale bar=80 μm.

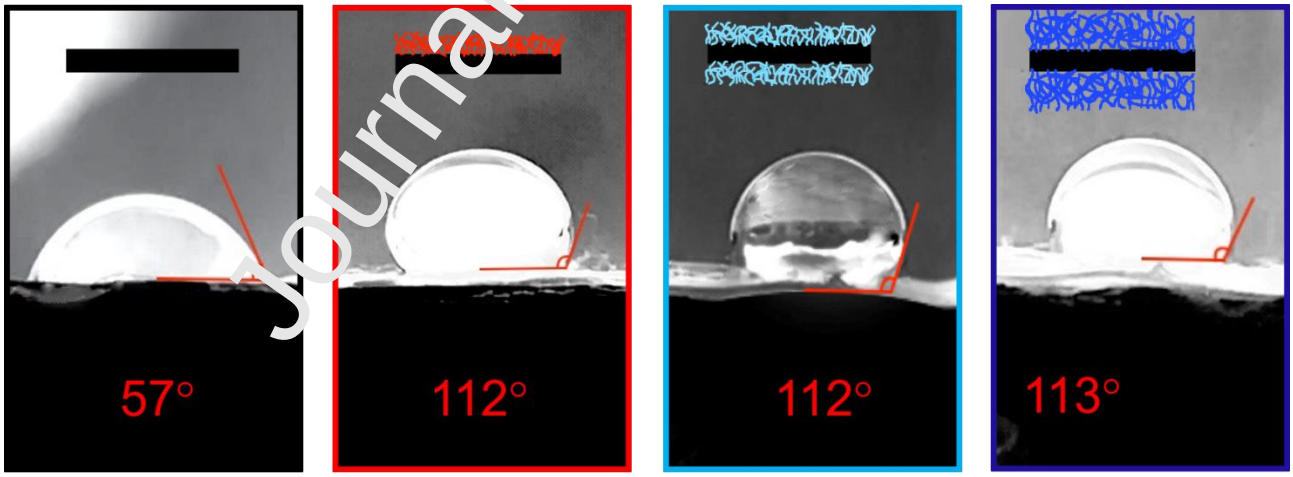

Figure 4. WCA of (from left to right) ML, BL, TL-5 and TL-10.

In order to detect possible changes in surface wettability, WCA measurements were performed and shown in **Figure 4**. ML displays a hydrophilic character (WCA=57°), due to the presence of CRV. In fact, WCA of neat PLA processed in the same way (sc-PLA) is equal to 74° (Fig. S3). The fibrous coating led to higher WCA values, which were found in the range 112-113 degrees. This feature was however

predictable, since – beyond the absence of CRV in electrospun membranes – the intrinsic roughness of fibrous structures is known to enhance the hydrophobicity [15].

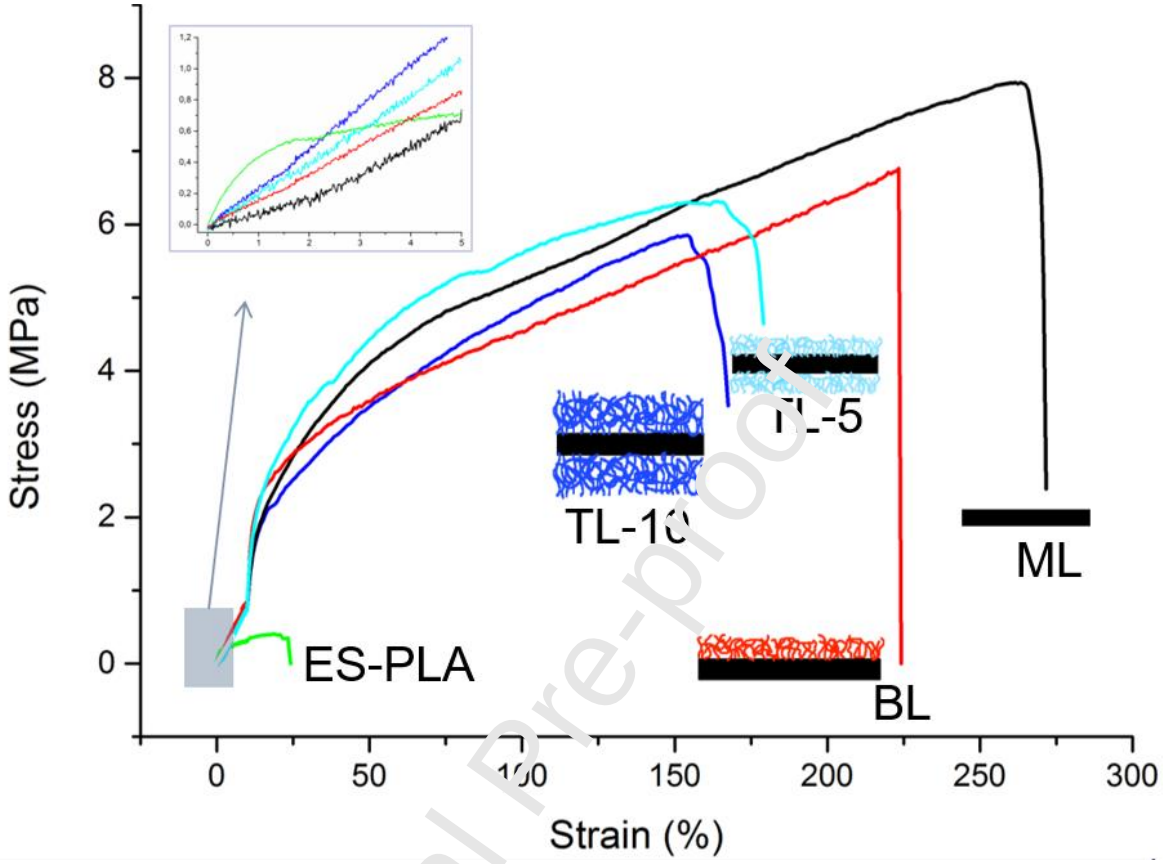

Figure 5. Representative stress-strain curves of ML, BL, TL-5 and TL-10, together with that of an electrospun PLA membrane (ES-PLA), as reference plot.

The representative stress-strain curves of ML, BL, TL-5 and TL-10 recorded during tensile tests are provided in **Figure 5**, together with that of an electrospun PLA membrane (ES-PLA) for sake of comparison. Basically, all the samples display a ductile behavior with a well-defined necking region and strain-hardening phenomena [16,17]. By analyzing the curves, it is possible to qualitatively assess that the stretchability tends to decrease upon increasing fibers/film ratio. In fact, being CRV contained in the inner dense layer only, this latter one is more ductile than neat sc-PLA (see Fig. S4), as expected, and even than fibrous mats. Therefore, stretchability decreases upon increasing the number of fibrous layers and their thickness (see again **Table 1**), with the effect of the less deformable ES-PLA mats becoming progressively more remarkable. Similarly, tensile strength values of fibrous membranes are typically much lower than those of dense films, because of obvious different density. A close-up of the low-strain region is provided in the inset of the same figure. ES-PLA displays the highest stiffness, while ML is the least rigid sample, due to the plasticizing effect of CRV. BL, TL-5 and TL-10 present elastic moduli

intermediate between those of ML and ES-PLA. In order to quantitatively assess the effect of combined processing onto the mechanical performance of such structures, the values of E, TS and EB derived from tensile tests have been reported in **Table 2**.

Table 2. Main tensile properties of the single and multilayer structures prepared

Sample	E (MPa)	TS (MPa)	EB (%)
ML	19.1 ± 3.0	7.54 ± 1.1	260 ± 35
BL	23.7 ± 3.2	5.95 ± 0.5	225 ± 40
TL-5	27.2 ± 4.1	5.84 ± 1.2	185 ± 20
TL-10	34.8 ± 4.8	6.01 ± 1.2	172 ± 25
ES-PLA	49.3± 4.7	0.8 ± 0.2	24 ± 4

Even in this case, stiffness was found to enhance upon increasing the contribution of fibrous PLA, with the ensuing decrease of CRV overall concentration. Beyond the differences observed, it is of enormous interest to note that breaking properties of BL, TL-5 and TL-10 laminates are substantially governed by the film layer, with this aspect being crucial in the perspective to couple the extremely high specific surface of fibrous surfaces with the higher mechanical performance of dense films.

Elastic modulus of laminates can be modeled by considering parallel slabs of material between platens that apply a load, assuming an *isostrain* condition, since each phase undergoes the same displacement. Under these hypotheses, each layer of the laminate gives a contribution to the composite stress that is proportional to the volume fraction of the phase and, therefore, the elastic modulus of the composite is given by the arithmetic mean of the moduli of each layer, weighted by the volume fractions. The elastic moduli experimentally measured were plotted as a function of volume fraction (Φ_V) of fibrous layer(s) and compared with those predicted by isostrain model. The results are provided in **Figure 6**.

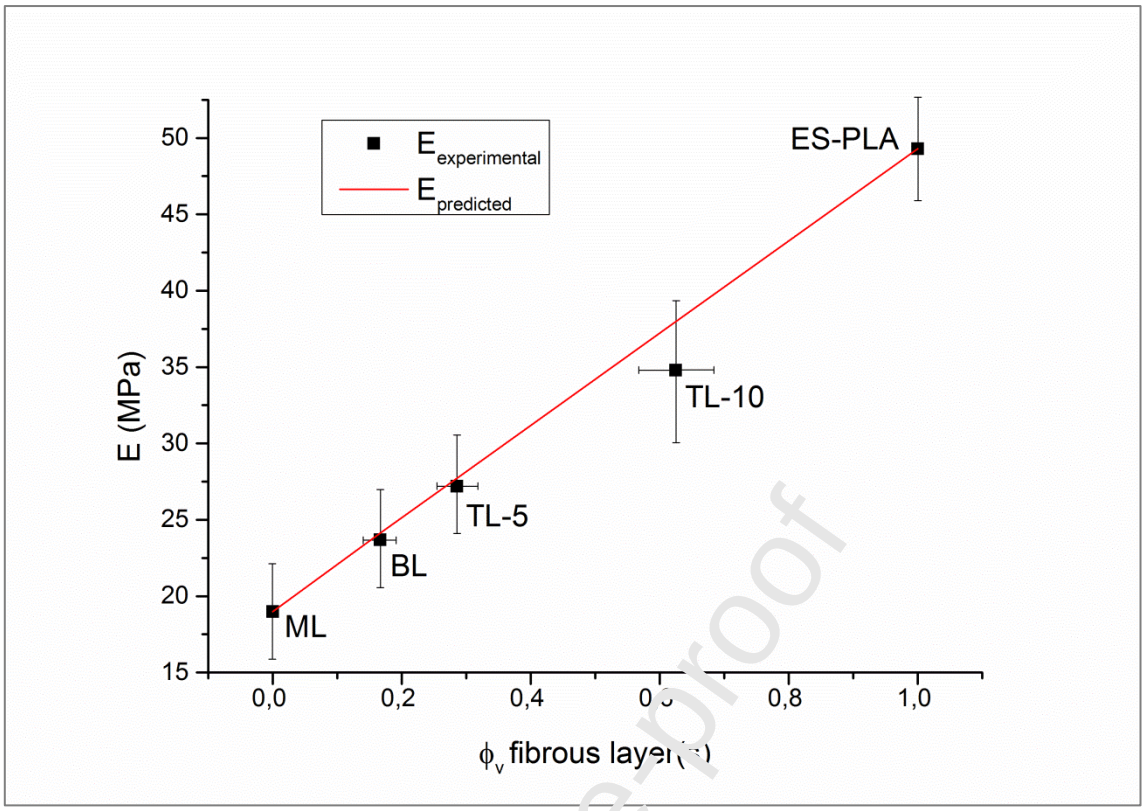

Figure 6. Comparison between experimental and predicted values of elastic modulus, plotted as a function of volume fraction (Φ_V) of fibrous layer(s).

Isostrain model allows predicting modulus of laminates with a high accuracy level, with this feature suggesting a good interlayer adhesion in the laminates, already envisaged by the uniform morphology of interfaces detected by SEM analysis (see again **Figure 2**). Elastic modulus of TL-10 was slightly lower than that predicted, however even in this latter case, the interlayer adhesion was found to be quite strong.

FTIR/ATR analysis was carried out with the purpose to detect the presence of CRV. FTIR spectra collected in the range 4000-400 cm^{-1} are shown in **Figure 7A**. In fact, although all the samples display the characteristic bands of PLA, such as those centered at 1750 cm^{-1} and 1150-1000 cm^{-1}, respectively referring to C=O and C-O stretching, it is possible to recognize the eventual presence of CRV by monitoring the band centered at 814 cm^{-1}, which is ascribed to CRV aromatic ring [9]. The magnification of this spectral region is provided in **Figure 7B**. Notably, the absorbance of such band was found to be more intense in ML, while decreasing for BL and TL-5, which displayed the same intensity value (note that for BL the analysis was performed onto fibrous layer, as indicated by the arrow in the pictorial representation inserted to the right of the panel). In TL-10, no characteristic peak of CRV could be detected. These data can be explained by considering two factors: firstly, ATR is a surface

characterization, whose depth penetration capability is reasonably lower than fibrous layer thickness of TL-10 [18]; secondly, although all the samples contain the same amount of CRV per unit of surface, being equal the middle layer, it is obvious that, upon increasing the volume of fibrous coating made by PLA only, CRV concentration tends to decrease, progressively going from 14% (ML) to about 4% (TL-10).

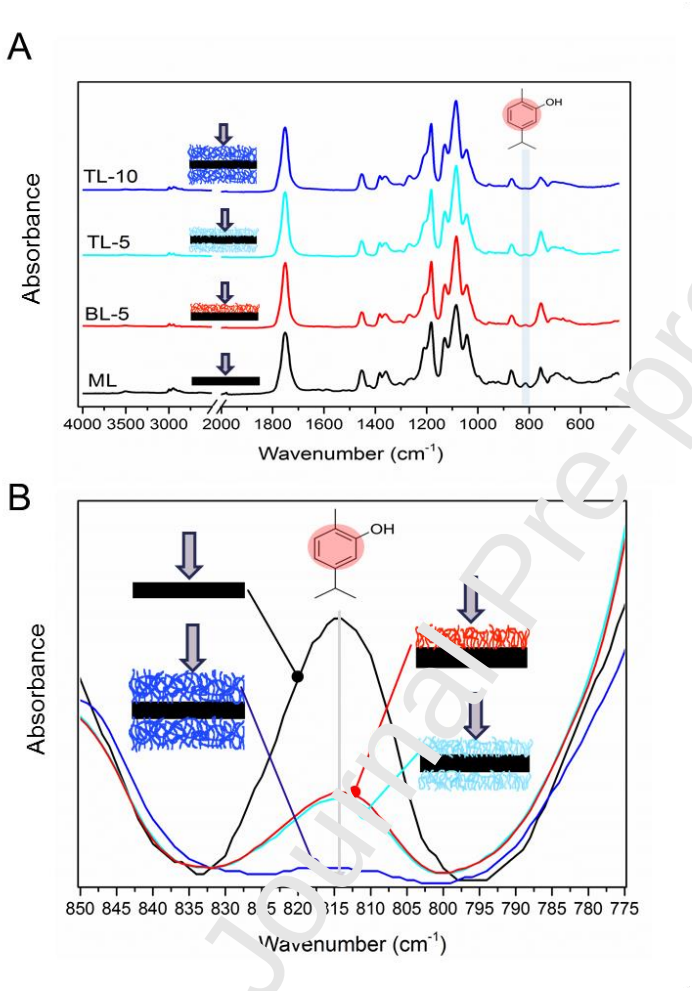

Figure 7. FTIR/ATR spectra (A) and close-up of the spectral range 850-775 cm^{-1} (B) collected for ML (black), BL (red), TL-5 (light blue) and TL-10 (blue). Note that measurements were performed onto the side indicated by the arrows.

The ability of the samples in providing controlled release of CRV was investigated by monitoring UV absorption wavelength at 273 nm of CRV at various time intervals [9].

Figure 8 provides the cumulative release of CRV expressed as M_t/M_{loaded} ratio upon immersion time, with M_t and M_{loaded} indicating respectively the amount of CRV released at a given time t, and the theoretical amount of CRV integrated into the devices, according to their formulation, reported in Table 1.

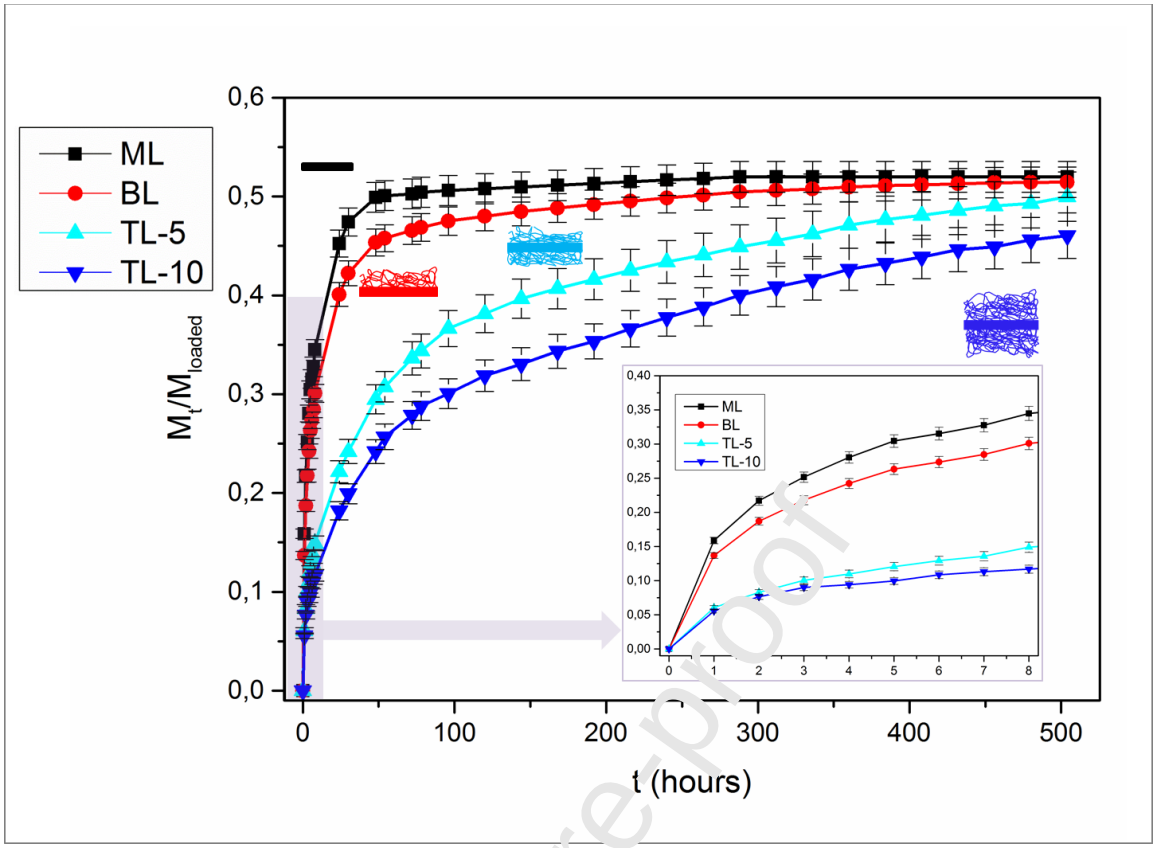

Figure 8. Release curves of ML, BL, TL-5 and TL-10 expressed as M_t/M_{loaded} as a function of time. Inset: close-up of the "burst" zone.

ML displays the typical release behavior of thin films, characterized by a burst in the early portion of the curves, when the driving force is higher, and a subsequent plateau, associated to the progressive depletion of CRV after a certain time interval. It is worth noting that after 300 hours any release activity was no longer observed.

Therefore, the maximum amount of CRV released was about only 50% of the theoretical loaded amount, i.e. the CRV initially added to the polymer solution used for solvent casting. This apparent discrepancy between loaded and released content is generally observed in polymeric systems containing essential oils, due to the volatilization of CRV during processing, and given the fact that a certain aliquot of CRV molecules remains entrapped within the structure [9,19,20]. When compared to ML, BL shows a substantially similar release behavior, being however characterized by a slightly lower burst release and a less pronounced leveling off at higher time intervals, since M_t/M_{loaded} is shown to monotonically increase, although slowly, for the entire time investigated, thus asymptotically tending to the saturation value achieved by ML. TL-5 and TL-10 exhibit a progressively reduction of burst release with ensuing

enhanced ability to retain a remarkably sustained release over the whole time investigated. Notably, none of them achieved any plateau until 550 hours.

Aiming at a closer inspection of release mechanism, experimental data were fitted according to Peppas-Korsmeyer model [21–24]:

$$\frac{M_t}{M_\infty} = kt^n \qquad (1)$$

Where t is the release time, k is a kinetic constant related to the properties of the drug delivery system, and n is the diffusion exponent that is an indicator about the release mechanism.

M_∞ is the mass delivered at the depletion time, usually calculated as the value of cumulative mass released at saturation [21–24]. Within the experimental time investigated, ML and BL have been the only samples that displayed a plateau, with M_∞ being equal to about 30% with respect to the loaded amount of CRV, while depletion time of TL-5 and TL-10 reasonably exceeds 550 hours. Therefore, the value of M_t/M_{loaded} calculated at saturation for ML and BL was taken as reference M_∞ for all the samples and the curves were normalized consequently.

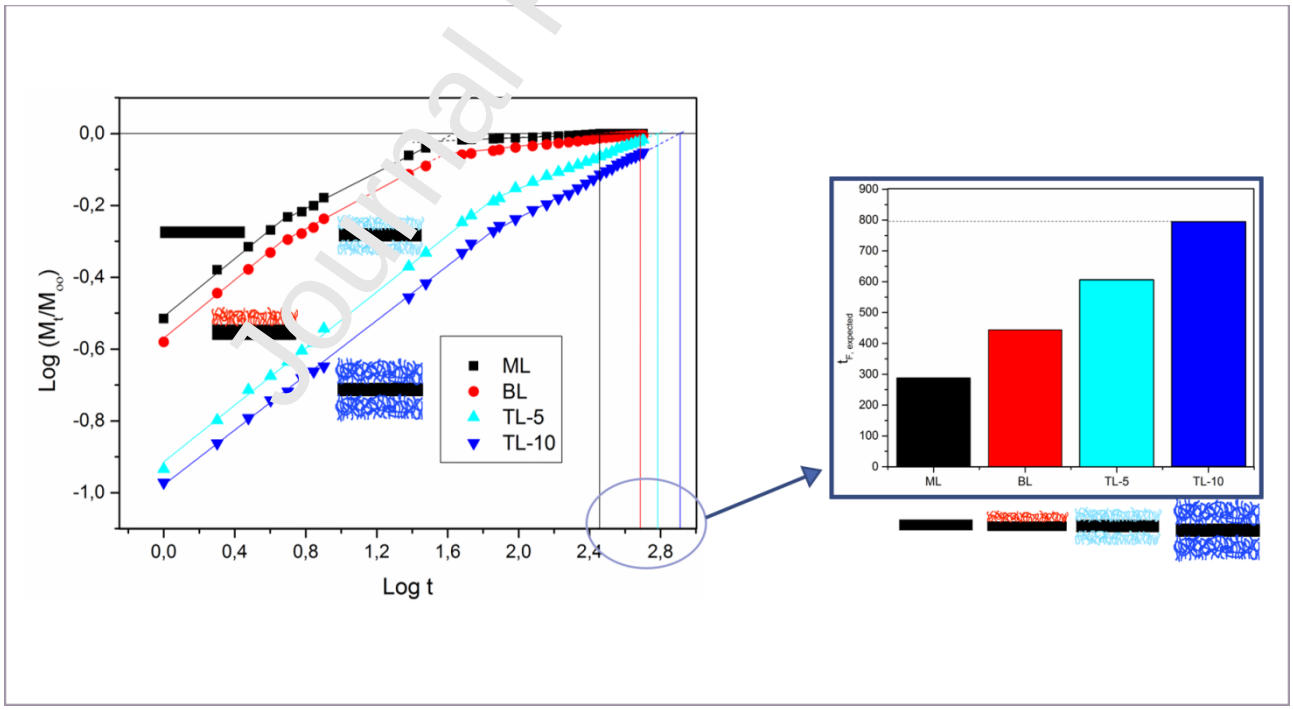

Figure 9. Release kinetics fitted according to Peppas-Korsmeyer model, together with the expected depletion time.

Figure 9 provides log M_t/M_∞ plotted as a function of log time for each sample. The release data were fitted by using Equation (1) until a satisfactory R^2 value (>0.99) was reached [25].

It is worth noting that Peppas-Korsmeyer model refers to the ideal condition of drug molecules homogeneously dispersed throughout the polymer matrix, and it is applicable only in the early portion of each curve, that is for M_t/M_∞<0.6 [26]. However, by analysing the slope and the intercept of the fitted lines in the first interval, it is possible to calculate n and k, respectively. The physical meaning of *n* provides information about the release mechanism, as listed in **Table 3**.

Table 3. Physical meaning of *n* exponent [24]

Release exponent (n) *	**Drug transport mechanism**
$n \leq 0.5$	Fickian diffusion (Case I)
$0.5 < n < 1.0$	Anomalous transport
n= 1.0 (**)	Case II transport
$n > 1.0$	Super case II transport

* for thin films, ** zero order release

Table 4. Main information provided by power model law fitting in the burst interval

Sample	Burst interval (Peppas-Korsmeyer)		
	n	k	R^2
ML	0.403	0.309	0.999
BL	0.405	0.271	0.999
TL-5	0.394	0.128	0.999
TL-10	0.380	0.118	0.999

As regards the burst interval, all the samples display a Fickian mechanism release with similar n values, while differing each other for the k values, which depend on the geometry of the samples [21–24]. Indeed, all the specimens possess the same diameter and substantially the same dense layer but different overall thickness. The analysis of k variation highlights that it is possible to easily control the release behavior by tailoring the features of fibrous surface of such samples.

Furthermore, the analysis of fitted lines in the last time range allows predicting the lifetime of each release device, with the expected depletion time being esteemed as the abscissa of the interception between the fitted line and the ordinate Log $\frac{M_t}{M_\infty} = 0$.

The predicted depletion times ($t_{F,\ expected}$) of the devices are reported in the right panel of **Figure 9**. Lifetime of ML was found to be 288 hours, whereas those expected for BL, TL-5 and TL-10 proved to be equal to 444, 607 and 795 hours, respectively. That is, 10 minutes (5 minutes for each side) or 20 minutes (10 minutes per side) of electrospinning are enough to double or even almost triple the lifetime of the release device.

A possible explanation of this interesting behavior could involve two phenomena:

(i) surface wettability was deeply affected by fibrous coating, which made the surface turn into hydrophobic, thus hindering the solvent penetration especially in the case of TL-10;

(ii) PLA microfibers adhered to the thin film thus serving as a capping agent, thereby forcing the carvacrol molecules to follow a more tortuous and longer path to leave the structure.

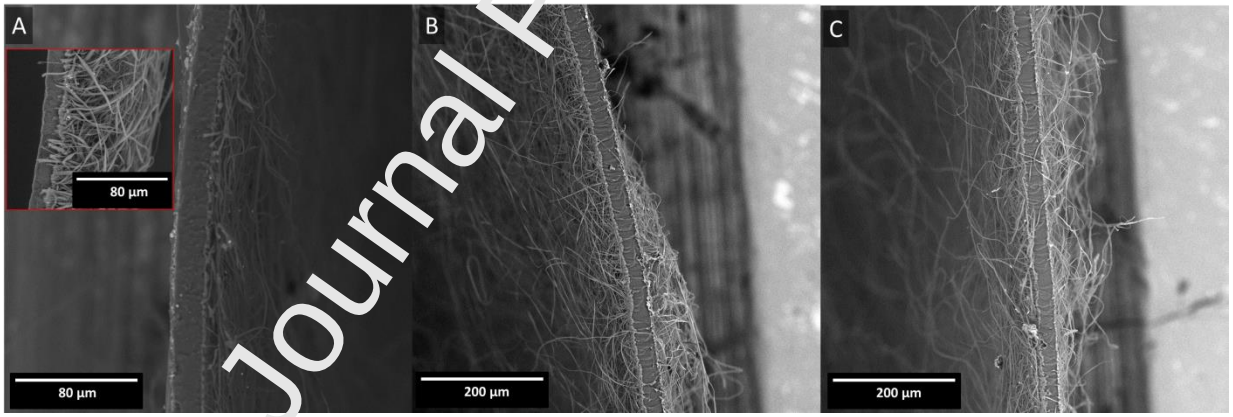

Figure 10. SEM micrographs of BL (A), TL-5 (B), TL-10 (D) after release tests. Inset of panel A points out the retention of uniform coverage of fibrous mats.

Aiming to investigate the durability of interlayer adhesion, the morphology of laminates after release tests was assessed. SEM micrographs of the laminate samples that underwent release tests, provided in **Figure 10**, put into evidence that the interlayer adhesion is retained after 550 h immersion, hence the outer layers are able to endow the materials with a durable hydrophobic layer which serves even as a capping agent, thus forcing CRV molecules to follow a longer path before being diffused out of the laminates. This feature is in fully agreement with the decrease of k values observed upon increasing the fibrous

component of the laminates. Moreover, the diffusion of CRV becomes progressively much more uniform upon increasing the contribution of fibrous layers. In fact, the fibrous layers, serving as a capping agent, are able to hinder the burst at the initial stage of release. Note that, in TL-10, the slope of Log $\frac{M_t}{M_\infty}$ proved to be almost constant within the entire time interval investigated, going from 0.381 (within the interval 0-56 hours) to 0.261 (56-550 hours), whereas ML was found unable to provide a sustained release above 24 hours.

Such prolonged release observed in this work was found to be much more remarkable than those reported in literature for three-layer systems during similar *in vitro* experiments [27,28]. Moreover, these results become even more relevant in the context of a volatile drug, such as CRV, which generally proves to be quickly delivered from either fibrous membranes (within 6-10 hours) [9] or dense film (288 hours) of PLA, but even when encapsulated in cyclodextrins [29] or complexed with graphene [9], no sustained release was observed after 100 hours. Indeed, long term release ability can be dramatically enhanced via the implementation of multi-step protocols, involving covalent immobilization routes, use and chemical modification of nanoparticles, drug encapsulation in engineered nanocarriers, thus leading to sustained release up to 40 days [30]. Of course, these latter methods, requiring time-consuming and high-cost operations, are preferable for durable implants and stents, whereas the technique proposed in this work, relying on a good compromise between cost-effectiveness/rapidity of manufacturing and long-time sustained release ability, might be useful for topical treating fungal and bacterial infections in external or interstitial tissues.

3. Conclusions

Electrospinning and solvent casting were coupled to achieve functionally graded laminates, comprising a thin film of polylactic acid, serving as a carvacrol reservoir, and one or two fibrous layers, herein used to modulate release kinetics of carvacrol. The presence of fibrous skin, especially in three-layer structures proved to progressively reduce the burst release at the early stage of immersion and to enhance the lifetime of release activity of such devices up to 800 hours. Furthermore, a correlation was found between the thickness of fibrous layers and release kinetics, thus suggesting that adjusting simple variables, such as electrospinning time allows a control of final properties and lifetime of these devices, which could be particularly promising for topical treatment of diseases and infections.

Moreover, this combined processing allows gathering the mechanical robustness of a dense film with the extremely large specific area of fibrous materials, thus showing promising potential in expanding applications of such materials. In fact, this simple assembly may be used to prepare membranes endowed with a consistent core, whose properties can be designed separately on demand, that may provide higher mechanical resistance and thus a long-term activity/reusability, while overcoming some typical drawbacks of electrospun membranes.

Acknowledgements:

This work has been partially funded by ZEROBrine project (European Union's Horizon 2020)

Credit author statement:

Roberto Scaffaro: Conceptualization, Investigation, Methodology, Supervision, Formal Analysis, Data Curation, Writing-Reviewing and Editing, Resources, Project administration.

Andrea Maio: Conceptualization, Investigation, Methodology, Formal analysis, Software, Visualization, Data Curation, Writing-Original draft preparation.

Emmanuel F Gulino: Investigation, Visualization, Data Curation, Software.

Giorgio DM Micale: Funding acquisition, Project administration, Writing-Reviewing and Editing.

Declaration of interests

The authors declare that they have no known competing financial interests or personal relationships that could have appeared to influence the work reported in this paper.

References

[1] T.-N. Gao, T. Wang, W. Wu, Y. Liu, Q. Huo, Z.-A. Qiao, S. Dai, Solvent-Induced Self-Assembly Strategy to Synthesize Well-Defined Hierarchically Porous Polymers, Adv. Mater. 31 (2019) 1806254. doi:10.1002/adma.201806254.

[2] F. Zhu, Q. Xin, Q. Feng, Y. Zhou, R. Liu, Novel poly(vinylidene fluoride)/thermoplastic polyester elastomer composite membrane prepared by the electrospinning of nanofibers onto a dense membrane substrate for protective textiles, J. Appl. Polym. Sci. 132 (2015). doi:10.1002/app.42170.

[3] J. Gao, B. Li, X. Huang, L. Wang, L. Lin, H. Wang, H. Xue, Electrically conductive and fluorine free superhydrophobic strain sensors based on SiO2/graphene-decorated electrospun nanofibers for human motion monitoring, Chem. Eng. J. (2019). doi:https://doi.org/10.1016/j.cej.2019.05.045.

[4] B.Q.H. Nguyen, A. Shanmugasundaram, T.-F. Hou, J. Park, D.-W. Lee, Realizing the flexible and transparent highly-hydrophobic film through siloxane functionalized polyurethane-acrylate micro-pattern, Chem. Eng. J. 373 (2019) 68–77. doi:https://doi.org/10.1016/j.cej.2019.04.197.

[5] K.J. De France, M. Babi, J. Vapaavuori, T. Hoare, J. Moran-Mirabal, E.D. Cranston, 2.5D Hierarchical Structuring of Nanocomposite Hydrogel Films Containing Cellulose Nanocrystals,

ACS Appl. Mater. Interfaces. 11 (2019) 6325–6335. doi:10.1021/acsami.8b16232.

[6] A. Maio, R. Scaffaro, L. Lentini, A. Palumbo Piccionello, I. Pibiri, Perfluorocarbons–graphene oxide nanoplatforms as biocompatible oxygen reservoirs, Chem. Eng. J. 334 (2018) 54–65. doi:10.1016/j.cej.2017.10.032.

[7] R. Scaffaro, F. Lopresti, A. Maio, F. Sutera, L. Botta, Development of polymeric functionally graded scaffolds: A brief review, J. Appl. Biomater. Funct. Mater. 15 (2017) 107–121. doi:10.5301/jabfm.5000332.

[8] R. Scaffaro, A. Maio, G. Lo Re, A. Parisi, A. Busacca, Advanced piezoresistive sensor achieved by amphiphilic nanointerfaces of graphene oxide and biodegradable polymer blends, Compos. Sci. Technol. 156 (2018) 166–176. doi:https://doi.org/10.1016/j.compscitech.2018.01.008.

[9] R. Scaffaro, A. Maio, F. Lopresti, Effect of graphene and fabrication technique on the release kinetics of carvacrol from polylactic acid, Compos. Sci. Technol. 169 (2019). doi:10.1016/j.compscitech.2018.11.003.

[10] T.J. Levingstone, E. Thompson, A. Matsiko, A. Schepens, J.P. Gleeson, F.J. O'brien, Multi-layered collagen-based scaffolds for osteochondral defect repair in rabbits, Acta Biomater. 32 (2016) 149–160. doi:10.1016/j.actbio.2015.12.034.

[11] P.K. Tripathi, B. Gorain, H. Choudhury, A. Srivastava, P. Kesharwani, Dendrimer entrapped microsponge gel of dithranol for effective topical treatment, Heliyon. 5 (2019) e01343. doi:https://doi.org/10.1016/j.heliyon.2019.e01343.

[12] N. Kusumaningrum, J.-H. Oh, D.H. Lee, C.-Y. Shin, J.-H. Jang, Y.K. Kim, J.H. Chung, Topical treatment with a cathepsin G inhibitor, β-keto-phosphonic acid, blocks ultraviolet irradiation-induced basement membrane damage in hairless mouse skin, Photodermatol. Photoimmunol. Photomed. 35 (2019) 148–156. doi:10.1111/phpp.12438.

[13] C.L. Nemeth, W.R. Lykins, H. Tran, M.E.H. ElSayed, T.A. Desai, Bottom-Up Fabrication of Multilayer Enteric Devices for the Oral Delivery of Peptides, Pharm. Res. 36 (2019) 89. doi:10.1007/s11095-019-2618-3.

[14] K. Nie, X. Yu, N. Kumar, Y. Zhan, Versatile Layer-By-Layer Highly Stable Multilayer Films: Study of the Loading and Release of FITC-Labeled Short Peptide in the Drug Delivery Field, Materials (Basel). 12 (2019). doi:10.3390/ma12081206.

[15] W.S. Choi, G.H. Kim, J.H. Shin, G. Lim, T. An, Electrospinning onto Insulating Substrates by Controlling Surface Wettability and Humidity, Nanoscale Res. Lett. 12 (2017). doi:10.1186/s11671-017-2300-6.

[16] R. Scaffaro, A. Maio, Integrated ternary bionanocomposites with superior mechanical performance via the synergistic role of graphene and plasma treated carbon nanotubes, Compos. Part B Eng. 168 (2019) 550–559. doi:https://doi.org/10.1016/j.compositesb.2019.03.076.

[17] R. Scaffaro, A. Maio, A green method to prepare nanosilica modified graphene oxide to inhibit nanoparticles re-aggregation during melt processing, Chem. Eng. J. 308 (2017) 1034–1047. doi:http://dx.doi.org/10.1016/j.cej.2016.09.131.

[18] R. Scaffaro, A. Maio, Influence of Oxidation Level of Graphene Oxide on the Mechanical Performance and Photo-Oxidation Resistance of a Polyamide 6, Polymers (Basel). 11 (2019). doi:10.3390/polym11050857.

[19] R. Requena, M. Vargas, A. Chiralt, Obtaining antimicrobial bilayer starch and polyester-blend films with carvacrol, Food Hydrocoll. 83 (2018) 118–133. doi:https://doi.org/10.1016/j.foodhyd.2018.04.045.

[20] I. Armentano, E. Fortunati, N. Burgos, F. Dominici, F. Luzi, S. Fiori, A. Jiménez, K. Yoon, J. Ahn, S. Kang, J.M. Kenny, Bio-based PLA_PHB plasticized blend films: Processing and structural characterization, LWT - Food Sci. Technol. 64 (2015) 980–988. doi:10.1016/j.lwt.2015.06.032.

[21] R. Scaffaro, L. Botta, A. Maio, M.C. Mistretta, F.P. La Mantia, Effect of Graphene Nanoplatelets on the Physical and Antimicrobial Properties of Biopolymer-Based Nanocomposites, Materials

(Basel). 9 (2016) 351. doi:10.3390/ma9050351.

[22] N.R. Saha, G. Sarkar, I. Roy, D. Rana, A. Bhattacharyya, A. Adhikari, A. Mukhopadhyay, D. Chattopadhyay, Studies on methylcellulose/pectin/montmorillonite nanocomposite films and their application possibilities, Carbohydr. Polym. 136 (2016) 1218–1227. doi:https://doi.org/10.1016/j.carbpol.2015.10.046.

[23] L. Keawchaoon, R. Yoksan, Preparation, characterization and in vitro release study of carvacrol-loaded chitosan nanoparticles, Colloids Surfaces B Biointerfaces. 84 (2011) 163–171. doi:https://doi.org/10.1016/j.colsurfb.2010.12.031.

[24] P.L. Ritger, N.A. Peppas, A simple equation for description of solute release II. Fickian and anomalous release from swellable devices, J. Control. Release. 5 (1987) 37–42.

[25] R. Scaffaro, A. Maio, L. Botta, E.F. Gulino, D. Gulli, Tunable release of Chlorhexidine from Polycaprolactone-based filaments containing graphene nanoplatelets, Eur. Polym. J. 110 (2019) 221–232. doi:10.1016/j.eurpolymj.2018.11.031.

[26] M.V. Dias, M.M. Sousa, B.R.B. Lara, V.M. de Azevedo, N. de Fatima Ferreira Soares, S.V. Borges, F. Queiroz, Thermal and morphological properties and kinetics of diffusion of antimicrobial films on food and a simulant, Food Packag. Shelf Life. 16 (2018) 15–22. doi:https://doi.org/10.1016/j.fpsl.2018.01.007.

[27] A.I. Rezk, A.R. Unnithan, C.H. Park, C.S. Kim, Rational design of bone extracellular matrix mimicking tri-layered composite nanofibers for bone tissue regeneration, Chem. Eng. J. 350 (2018) 812–823. doi:https://doi.org/10.1016/j.cej.2018.05.185.

[28] S. Vakilian, S. Mashayekhan, I. Shabani, M. Khorashadizadeh, A. Fallah, M. Soleimani, Structural stability and sustained release of protein from a multilayer nanofiber/nanoparticle composite, Int. J. Biol. Macromol. 75 (2015) 248–257. doi:https://doi.org/10.1016/j.ijbiomac.2015.01.051.

[29] D.O. Castro, N. Tabary, B. Martel, A. Gandini, N. Belgacem, J. Bras, Effect of different carboxylic acids in cyclodextrin functionalization of cellulose nanocrystals for prolonged release of carvacrol, Mater. Sci. Eng. C. 69 (2016) 1018–1025. doi:https://doi.org/10.1016/j.msec.2016.08.014.

[30] L.-Y. Huang, M.-C. Yang, H.-M. Tsou, T.-Y. Liu, Hemocompatibility and anti-fouling behavior of multilayer biopolymers immobilized on gold-thiolized drug-eluting cardiovascular stents, Colloids Surfaces B Biointerfaces. 173 (2019) 470–477. doi:https://doi.org/10.1016/j.colsurfb.2018.10.014.

Graphical abstract:

Highlights

- We designed a combined processing approach coupling electrospinning and film casting;
- We achieved laminates comprising a dense PLA-carvacrol layer and fibrous PLA skins;
- This approach allows devices with tunable properties by controlling the process;
- Graded laminates gather high mechanical performance and tunable carvacrol release;
- Combined processing approach can be easily extended to other processes and materials.

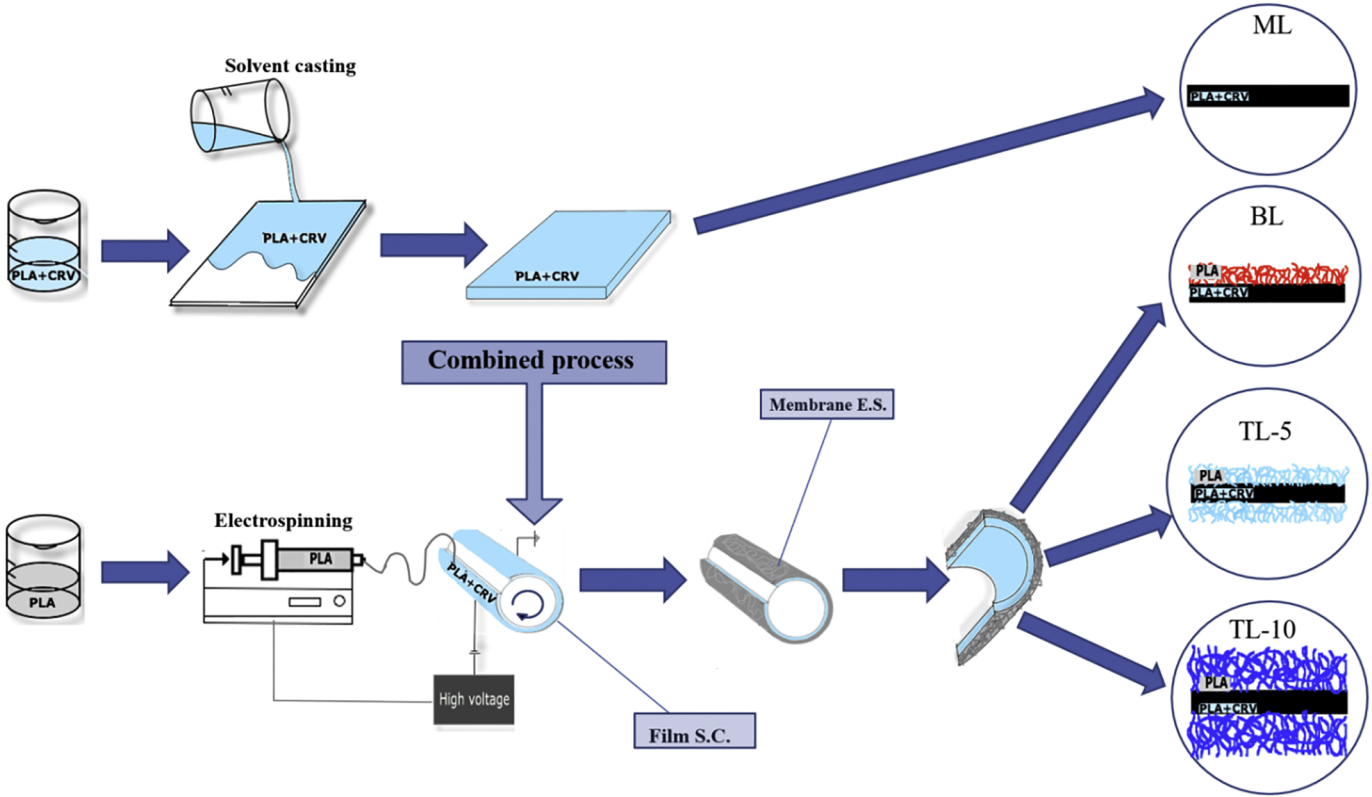
Solvent casting
PLA+CRV
PLA+CRV
PLA+CRV
ML
PLA+CRV
BL
PLA
PLA+CRV
Combined process
Membrane E.S.
TL-5
PLA
PLA+CRV
Electrospinning
PLA
PLA
PLA+CRV
TL-10
PLA
PLA+CRV
High voltage
Film S.C.

Figure 1

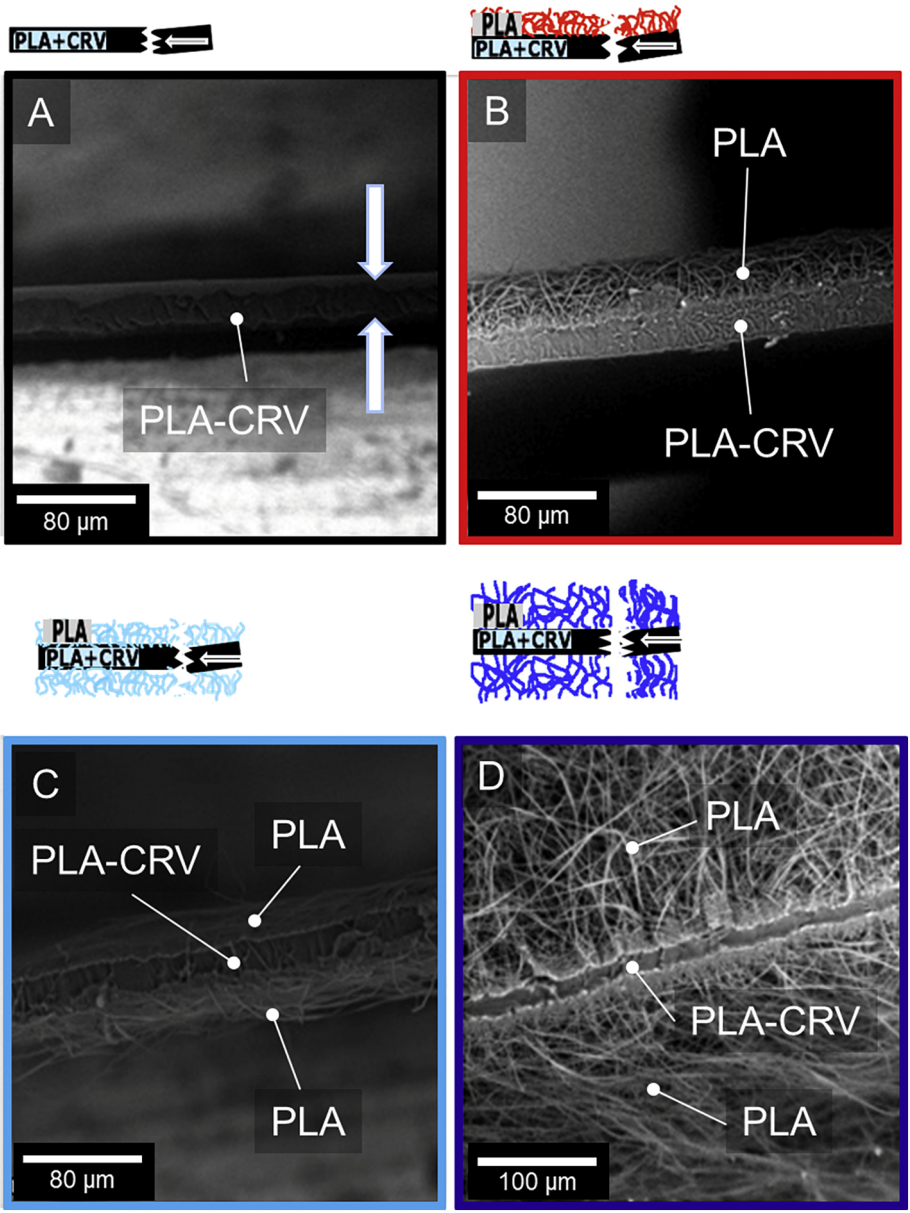
PLA+CRV
PLA
PLA+CRV
A
PLA-CRV
80 µm
B
PLA
PLA-CRV
80 µm
PLA
PLA+CRV
PLA
PLA+CRV
C
PLA-CRV
PLA
PLA
80 µm
D
PLA
PLA-CRV
PLA
100 µm

Figure 2

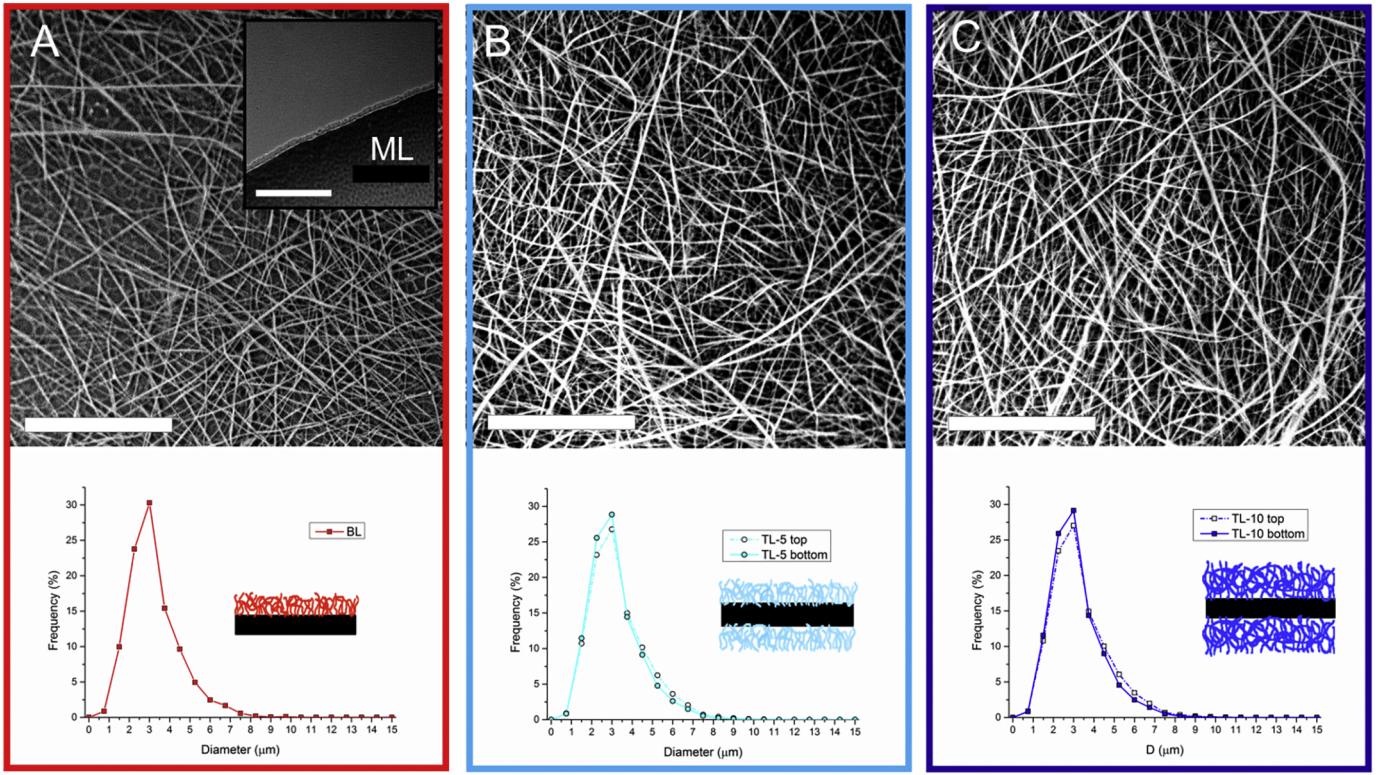
A
ML
B
C
Frequency (%)
Diameter (μm)
BL
TL-5 top
TL-5 bottom
TL-10 top
TL-10 bottom
D (μm)

Figure 3

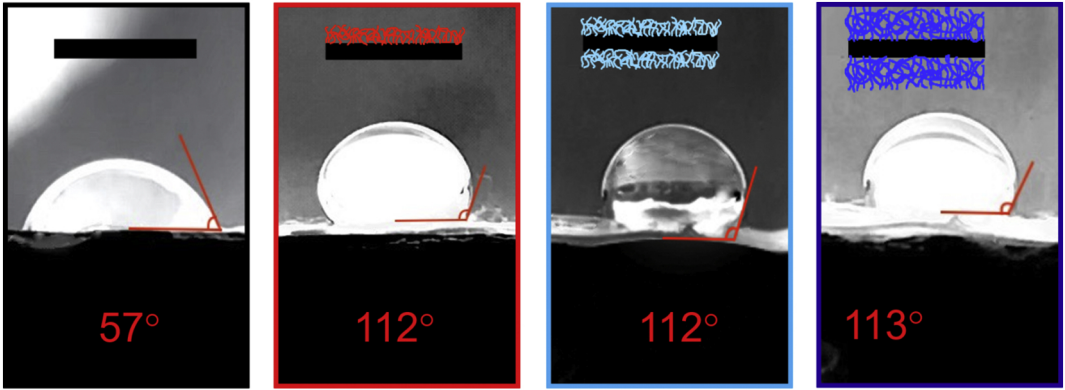

Figure 4

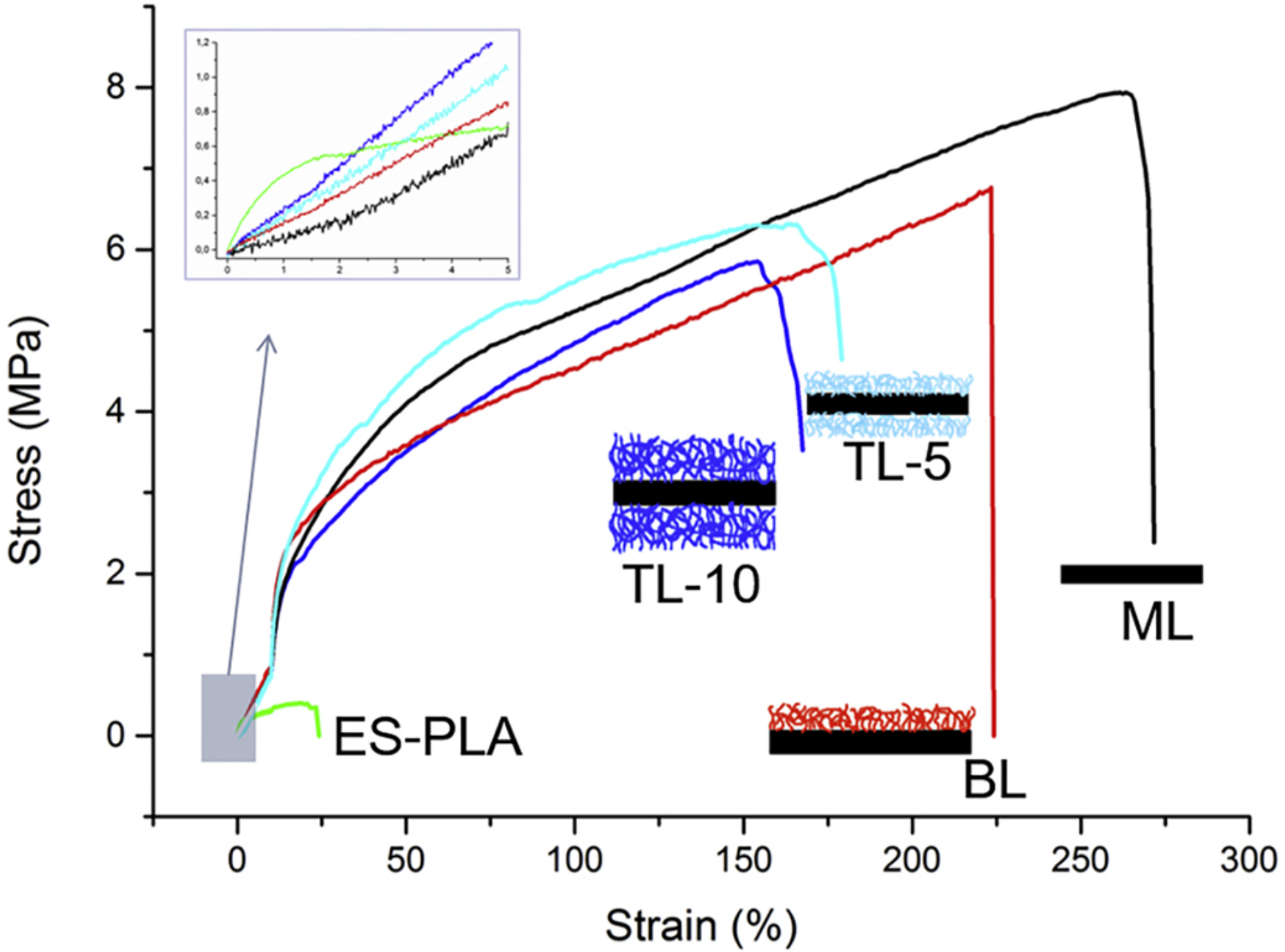
Stress (MPa)
Strain (%)
0
2
4
6
8
0
50
100
150
200
250
300
ES-PLA
TL-10
TL-5
BL
ML

Figure 5

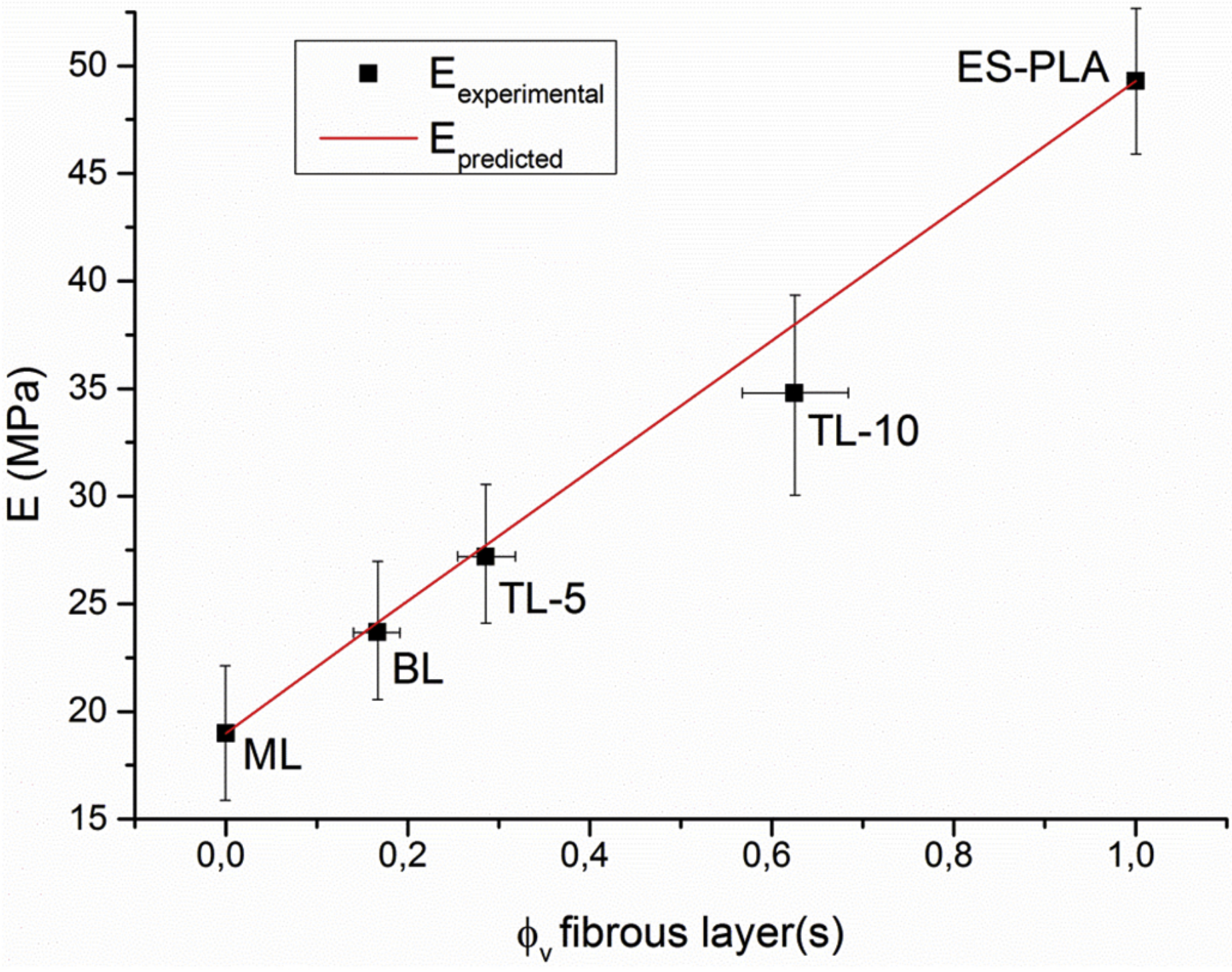
E experimental
E predicted
ES-PLA
TL-10
TL-5
BL
ML
E (MPa)
50
45
40
35
30
25
20
15
0,0
0,2
0,4
0,6
0,8
1,0
ϕv fibrous layer(s)

Figure 6

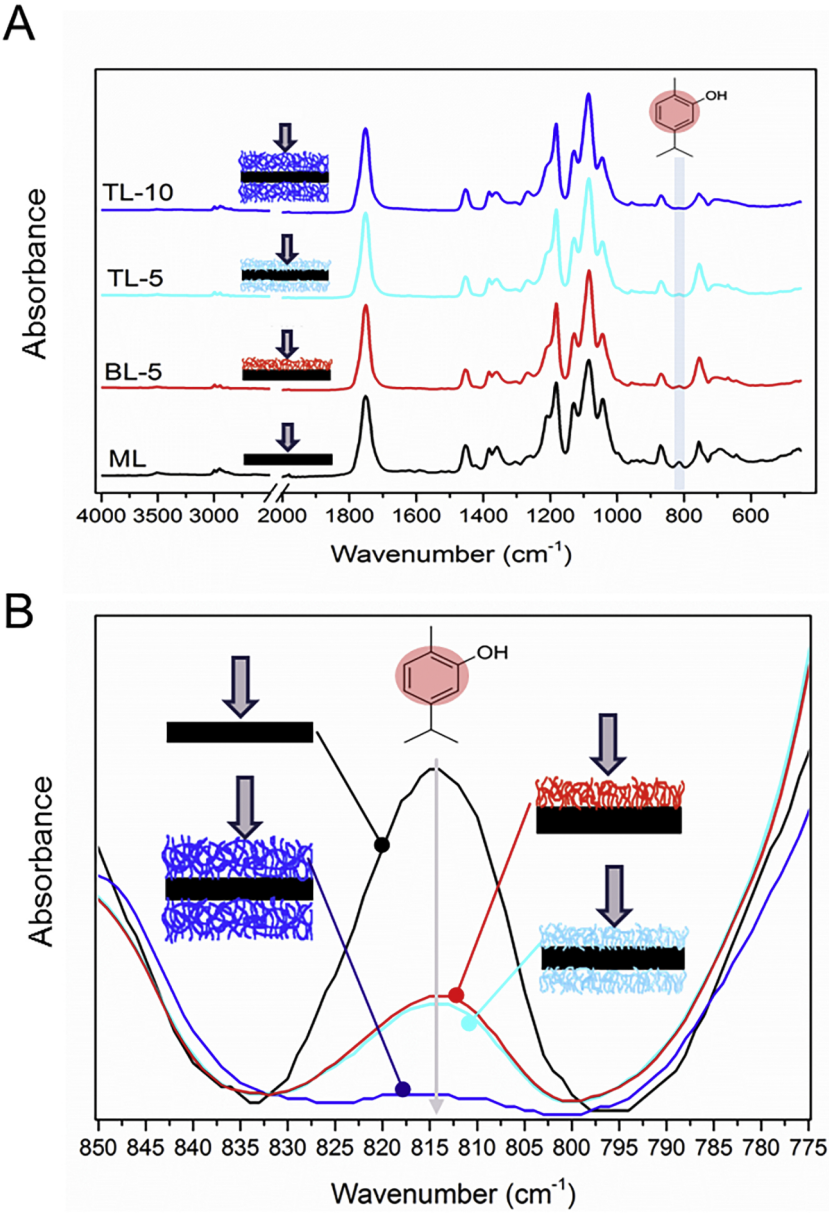
A
Absorbance
TL-10
TL-5
BL-5
ML
OH
4000 3500 3000 2000 1800 1600 1400 1200 1000 800 600
Wavenumber (cm-1)
B
Absorbance
OH
850 845 840 835 830 825 820 815 810 805 800 795 790 785 780 775
Wavenumber (cm-1)

Figure 7

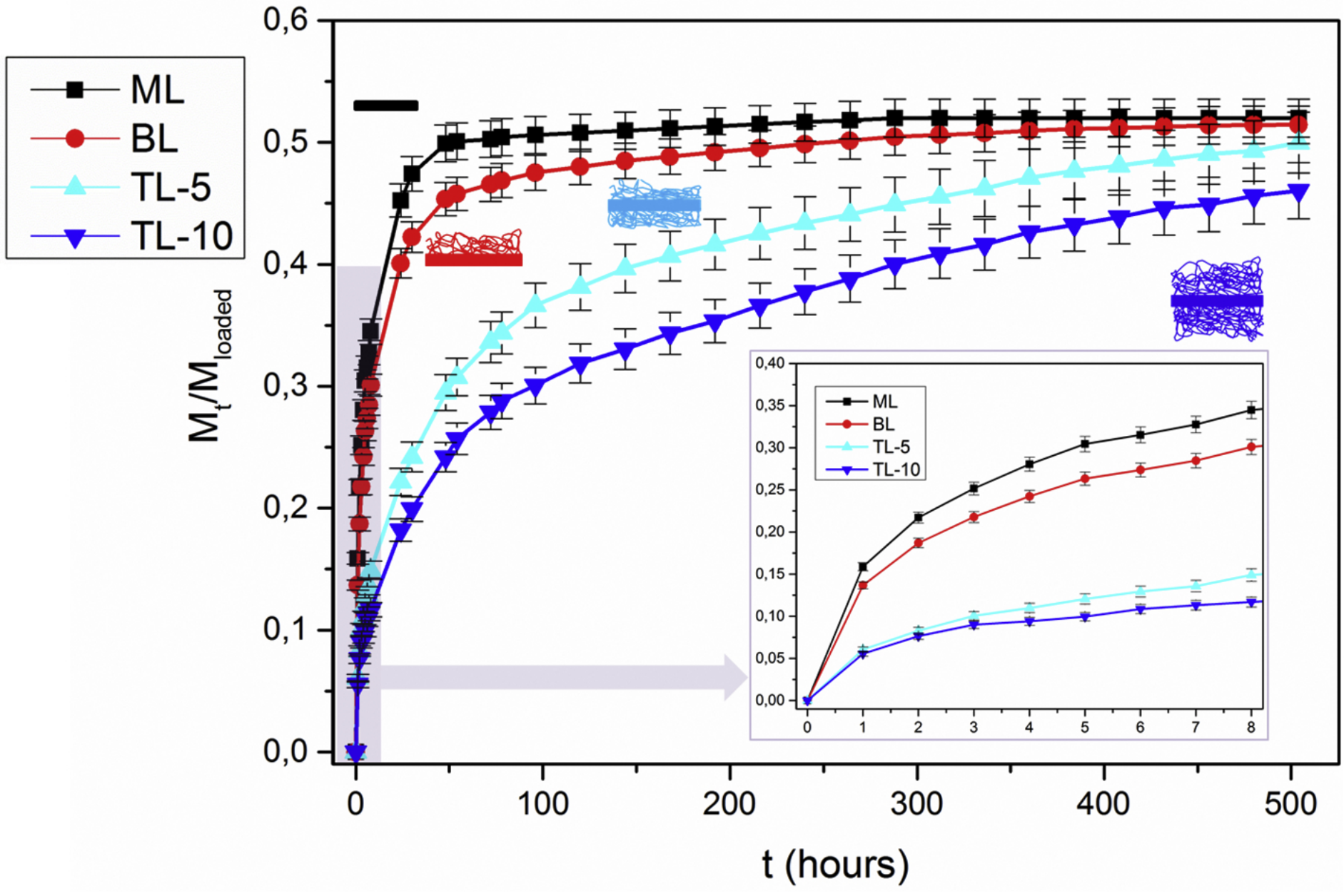
ML
BL
TL-5
TL-10
M_t/M_{loaded}
t (hours)
0,0
0,1
0,2
0,3
0,4
0,5
0,6
0
100
200
300
400
500
0,00
0,05
0,10
0,15
0,20
0,25
0,30
0,35
0,40
0
1
2
3
4
5
6
7
8

Figure 8

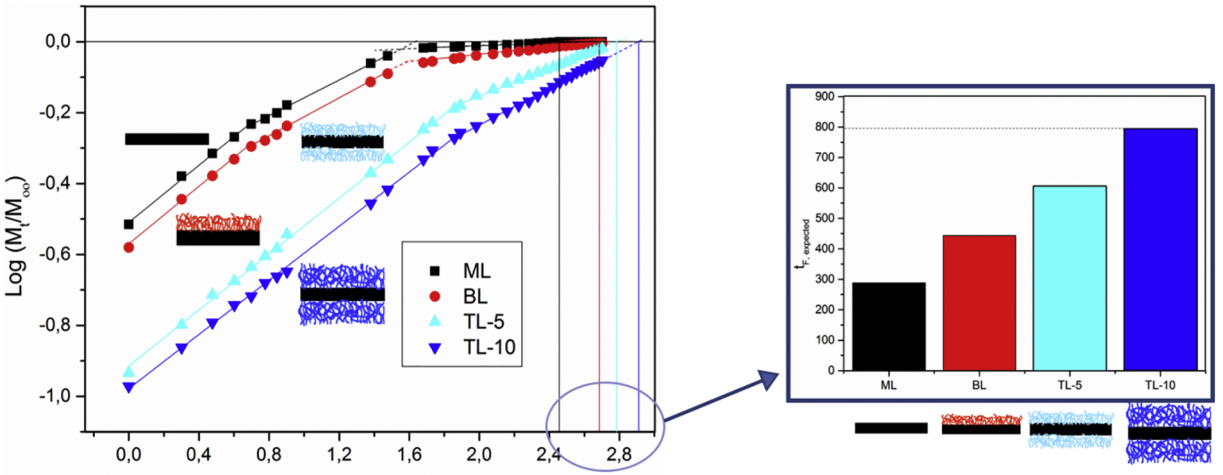
0,0
-0,2
-0,4
-0,6
-0,8
-1,0
Log (M_t/M_∞)
0,0
0,4
0,8
1,2
1,6
2,0
2,4
2,8
Log t
ML
BL
TL-5
TL-10
900
800
700
600
500
400
300
200
100
0
t_F, expected
ML
BL
TL-5
TL-10

Figure 9

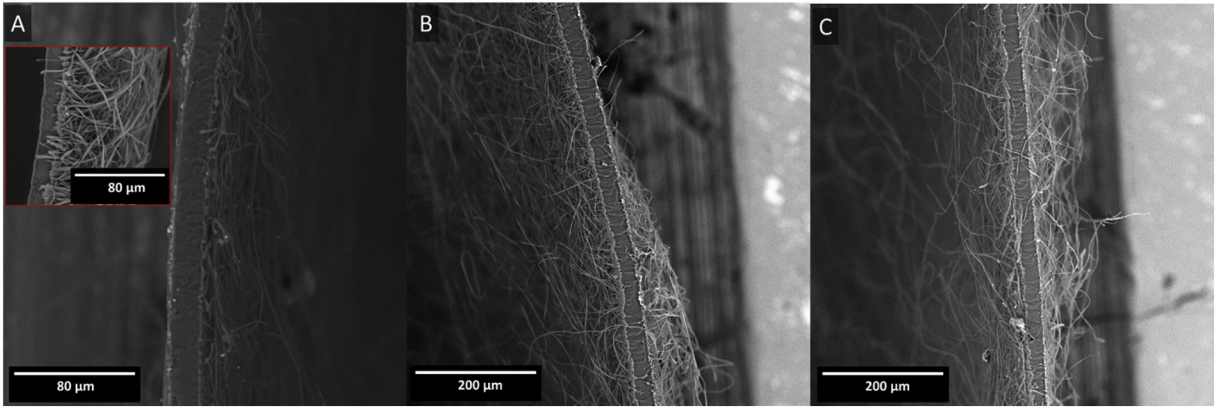

Figure 10